UDK 669.15:539.4.016:621.785
Original scientific article/Izvirni znanstveni članek

ISSN 1580-2949
MTAEC9, 56(2)233(2022)

INFLUENCE OF HEAT TREATMENT ON THE HIGH-TEMPERATURE OXIDATION BEHAVIOUR OF CHROMIUM-MOLYBDENUM-VANADIUM ALLOYED HOT-WORK TOOL STEEL

VPLIV TOPLOTNE OBDELAVE NA VISOKO TEMPERATURNO OKSIDACIJO KROM-MOLIBDEN-VANADIJ ORODNEGA JEKLA ZA DELO V VROČEM

Tilen Balaško[1], Maja Vončina[1], Jaka Burja[1,2], Jožef Medved[1]

[1]Faculty of Natural Sciences and Engineering, University of Ljubljana, Aškerčeva cesta 12, 1000 Ljubljana, Slovenia
[2]Institute of Metals and Technology, Lepi pot 11, 1000 Ljubljana, Slovenia

Prejem rokopisa – received: 2026-02-16; sprejem za objavo – accepted for publication: 2022-03-09

doi:10.17222/mit.2022.406

The high-temperature oxidation behaviour of chromium-molybdenum-vanadium alloyed hot-work tool steel was investigated. High-temperature oxidation was investigated in two conditions: soft annealed, and quenched and tempered. The samples were oxidised in a chamber furnace and in an instrument for simultaneous thermal analysis, for 100 h in the temperature range between 400 °C and 700 °C. Metallographic analysis (optical and scanning electron microscopy) was performed to study the microstructural changes in the steel and the oxide layer. Oxidation kinetics were analysed by thermogravimetric analysis, and equations were derived from the results. The kinetics can be described by three mathematical functions, namely: exponential, parabolic and cubic. However, which function best describes the kinetics depends on the oxidation temperature and the thermal condition of the steel. Quenched and tempered samples were shown to oxidise less, resulting in a slower oxidation rate.

Keywords: heat treatment, tool steel, oxidation, thermogravimetric analysis

Izvedena je bila raziskava visokotemperaturne oksidacije krom-molibden-vanadijevega orodnega jekla za delo v vročem. Raziskave visokotemperaturne oksidacije so bile opravljene na vzorcih jekla v mehko žarjenem stanju in na vzorcih v poboljšanem stanju. Oksidacija vzorcev je potekala 100 ur v komorni peči in v STA (simultana termična analiza) napravi v temperaturnem območju med 400 °C in 700 °C. Identifikacija mikrostrukturnih sprememb v vzorcih in oksidne plasti je bila izvedena z metalografsko analizo (optična in vrstična elektronska mikroskopija). Kinetika oksidacije je bila opazovana s termo-gravimetrično analizo. Iz rezultatov preizkusov so bile izpeljane matematične enačbe za opis visokotemperaturne oksidacijske kinetike. Kinetika se lahko opiše s tremi matematičnimi funkcijami eksponentno, parabolično in kubično. Katera funkcija pa najbolje opisuje kinetiko, je odvisno od temperature oksidacije in toplotnega stanja jekla. Dokazano je, da poboljšani vzorci manj oksidirajo, kar ima za posledico počasnejšo hitrost oksidacije.

Ključne besede: toplotna obdelava, orodno jeklo, oksidacija, termo-gravimetrična analiza

1 INTRODUCTION

Dievar is a chromium-molybdenum-vanadium alloyed hot-work tool steel that belongs to the group of chromium hot-work tool steels. They are most commonly used to make tools and dies for high-pressure die casting and forging.[1–3] Since hot-work tool steels are normally used at elevated temperatures, the high-temperature oxidation behaviour is of great importance. The effects of elevated temperatures on the properties of hot-work tool steels have been studied extensively.[4–10] The higher the temperature, the faster the tool steel degradation, mainly due to softening. But softening is not the only degradation mechanism; corrosion for instance can also play an important role in material degradation. Oxidation is an important type of corrosion, this is especially true for elevated temperatures. That is why we conducted a study of the high-temperature oxidation kinetics in the temperature range between 400 °C and 700 °C. Metals and alloys oxidise in air or other oxygen-containing atmospheres.[11–14] Oxygen in the gaseous state reacts with pure metals (M) to form oxides (M_aO_b) according to the chemical reaction:[12]

$$\frac{2a}{b}\,\mathrm{M(s)} + \mathrm{O_2(g)} \rightleftharpoons \frac{2}{b}\,\mathrm{M_aO_b(s)} \qquad (1)$$

The oxidation kinetics can follow several different laws, the most common of which are linear, parabolic, cubic, logarithmic and inverse logarithmic. In fact, kinetics is complex and can be described by a combination of several laws (linear and parabolic, etc.). The kinetics of the linear law can be described by the following Equation (2):[11–17]

$$\frac{\mathrm{d}\xi}{\mathrm{d}t} = f(t) \rightarrow \mathrm{d}\xi = \mathrm{d}n_{\mathrm{M_aO_b}} = -\frac{\mathrm{d}n_{\mathrm{M}}}{a} = -\frac{2\mathrm{d}n_{\mathrm{O_2}}}{b} \qquad (2)$$

*Corresponding author's e-mail:
tilen.balasko@ntf.uni-lj.si

Where ξ is a measure of the extent of the reaction at time t, n is the number of moles, M stands for the metal, O for oxygen, and a and b are the number of atoms in the oxide (M_aO_b).[11–17] Since oxidation kinetics is usually studied by a change in weight as a function of oxidation time, a parabolic law can be expressed by the Pilling-Bedworth Equation (3):[18,19]

$$\frac{dW}{dt} = k_p' W \quad \text{or} \quad W^2 = k_p t + W_0^2 \tag{3}$$

where W is the change in weight per unit area due to the oxidation of iron and k_p (= $2k_p'$) is the parabolic constant in $g^2 \cdot cm^{-4}$ sec^{-1}, and W_0 is the initial weight at the time (t = 0) of parabolic oxidation. In the original Pilling-Bedworth equation,[19] W_0 is equal to 0. On the other hand, the oxidation of iron below 700 °C is much more complex, as shown by the published results of different authors,[18,20–22] which differ greatly. In previous studies, it was found that the kinetics of the isothermal oxidation of iron in the temperature range 570–700 °C follows a parabolic law. However, the thicknesses of the individual oxide layers differ from study to study.[18,19,23] There are some studies on the high-temperature oxidation of hot-work tool steels[24–27] that also gave a first insight into the high-temperature kinetics and the composition of the oxide layers formed.

2 EXPERIMENTAL PART

A chromium-molybdenum-vanadium alloyed hot-work tool steel with the chemical composition given in **Table 1**, measured by wet chemical analysis and infrared absorption after combustion with ELTRA CS-800, was investigated. The steel is produced by the manufacturer Uddeholm under the trade name Dievar.

The first heat treatment of the steel under investigation was carried out. The austenitization temperature was 1025 °C and the soaking time was 30 min. Then, quenching in oil was performed, followed by two-stage tempering at 550 °C and 630 °C for 2 h to achieve a hardness of 42–44 HRC. The heat treatment was carried out in a Bosio EUP-K 6/1200 chamber furnace. Because an air atmosphere was used, 2 mm of the steel surface was milled off due to decarburisation and oxidation during the heat treatment. Three different types of samples were produced. The first were cubes measuring (10 × 10 × 10) mm (length × width × height), which were used during the high-temperature oxidation in the chamber furnace. These samples were prepared for further analysis under the light microscope and scanning electron microscope (SEM). The second samples are cylinders with height h = 4 mm and diameter d = 4 mm, which were used during high-temperature oxidation in the NETZSCH STA (Simultaneous Thermal Analyzer) Jupiter 449C instrument. All the surfaces were polished with 1-µm polycrystalline diamond suspension.

In order to gain an initial insight into the microstructural composition of the steel under investigation, CALPHAD simulations (CALculation of PHAse Diagrams) were carried out with the Thermo-Calc software using the TCFE10 thermodynamic database (TCS Steel and Fe-alloys Database).[28] The thermo-Calc software and the HSC Chemistry 9.0 software were also used to calculate the Gibbs free energy of the oxidation reactions.

High-temperature oxidation was studied at (400, 500, 600, and 700) °C in an air atmosphere for 100 h. The samples analysed with a light microscope and SEM were oxidised in the Bosio EUP-K 6/1200 chamber furnace. The heating rate was 15 °C/min and the high-temperature oxidation was carried out in an air atmosphere. To improve the oxidation conditions, additional air (79 φ/% nitrogen, 21 φ/% oxygen, 0.9 φ/% argon and 0.1 φ/% hydrocarbons and other inert gases) was introduced into the furnace at a flow rate of 0.3 L/min. Cooling in the chamber furnace was at a cooling rate of 0.5 °C/min, which was intentionally slow. The main reason for this was to avoid damaging the oxide layer.

The samples used for the kinetics study were oxidised in the NETZSCH STA Jupiter 449C machine. The heating and cooling rates were 10 °C/min, and air was also injected into the furnace at a flow rate of 30 mL/min (during the heating/cooling segment and the isothermal segment). Thermogravimetric analysis (TGA) was used to study the kinetics.

The samples for the SEM analysis were ground and polished. A field-emission-gun scanning electron microscope (FEG-SEM) ThermoFisher Scientific Quattro S was used to study the thickness of the oxide layers. For light microscopy, the samples were also ground, polished and etched with Vilella reagent. A Microphot FXA, Nikon with 3CCD video camera Hitachi HV-C20A was used for microstructural analysis. Vickers hardness was measured using an Instron Tukon 2100B. As the samples were examined in two different conditions, i.e., soft annealed, and quenched and tempered, the first were marked Dievar (soft annealed) and the second Dievar-HT (heat treated – quenched and double tempered).

3 RESULTS AND DISCUSSION

3.1 CALPHAD simulations

In order to show which phases are thermodynamically stable in the steel under investigation, a CALPHAD analysis was used. The calculated amount of thermody-

Table 1: Chemical composition of investigated Dievar hot-work tool steel given (w/%)

Sample	C	Si	Mn	P	S	Cr	Ni	Mo	V	Fe
Dievar	0.34	0.17	0.44	0.008	0.001	5.05	0.19	2.37	0.54	bal.

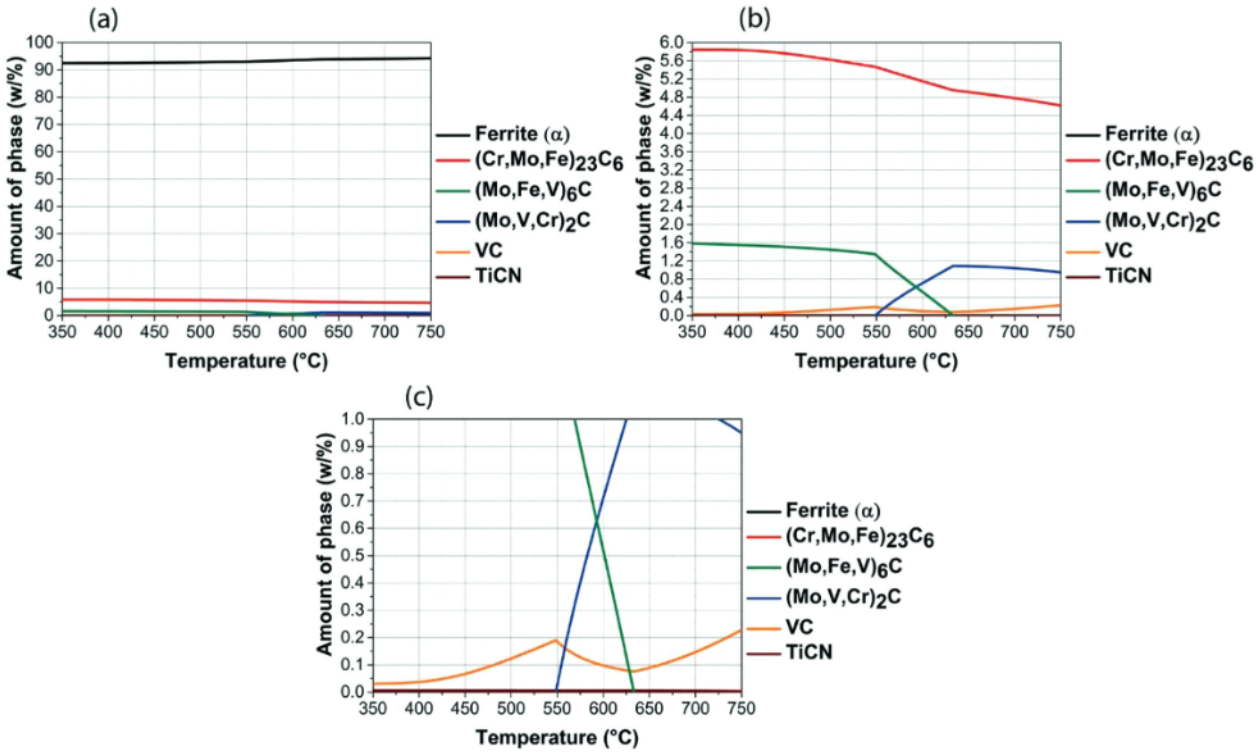

Figure 1: Amount of all thermodynamically stable equilibrium phases as a function of temperature for Dievar steel

namically equilibrium stable phases for the steels studied is shown in **Figure 1**. Considering only the carbides, the Dievar steel (**Figures 1a** to **1c**) consists of carbides $M_{23}C_6$ ($(Cr,Mo,Fe)_{23}C_6$), M_6C ($(Mo,Fe,V)_6C$) and M_2C ($(Mo,V,Cr)_2C$) as well as small amounts of VC and TiCN in the temperature range studied. There is also a transformation at 550 °C where M_6C ($(Mo,Fe,V)_6C$) carbides start to transform into M_2C ($(Mo,V,Cr)_2C$) carbides, which ends at 630 °C.

3.2 Thermogravimetric analysis

Thermogravimetric analyses were used to measure the change in weight of the samples during high-temperature oxidation. The kinetics of high-temperature oxidation for the steel studied was described by mathematical functions. For the best fit of the actual TGA curves to the mathematical functions, we used an iterative rectangular distance regression algorithm. Equations describing the change in weight of the sample per unit area over time for each temperature are also presented for each sample studied. Since we tried to simulate real conditions, we blew air into the furnace during the heating of the samples in the STA device, the TGA curve in the heating segment differs from that under isothermal conditions. Therefore, we described each TGA curve with two equations, the first giving the oxidation kinetics during heating and the second giving the oxidation kinetics under isothermal conditions. To describe the TGA curves, we used a two-phase and a single-phase exponential growth function (Equations (4) and (5)), a second-degree polynomial (Equation (6) – parabolic law) and a third-degree polynomial (Equation (7) – cubic law).

$$W\left(\frac{\Delta m}{A}\right) = y = Ae^{t/B} + Ce^{t/D} + E \tag{4}$$

$$W\left(\frac{\Delta m}{A}\right) = y = Ae^{t/B} + E \tag{5}$$

$$W\left(\frac{\Delta m}{A}\right) = y = A + Bt + Ct^2 \tag{6}$$

$$W\left(\frac{\Delta m}{A}\right) = y = A + Bt + Ct^2 + Dt^3 \tag{7}$$

In all cases, t is the time, Δm is the change in weight, A is the specific surface area of the sample, while the other coefficients depend on the temperature and chemical composition of the steel. The rate constants (k_n) were calculated for all the samples investigated and for both parts of the TGA curve after Equation (8) was derived by simple linear regression. The basic equation for calculating the rate constant (k_n) is as follows:

$$\left(\frac{\Delta m}{A}\right)^n = k_n t \tag{8}$$

where Δm is the change in weight in mg, A is the specific surface area in cm^2, t is the oxidation time in s and k_n is the rate constant, where n can be 1, 2 or 3 in the case of a linear, parabolic or cubic law, respectively. In the case of the exponential law, $1 < n < 3$. The index n was named after the type of equation, so that the expo-

nential law has the index *e*, the parabolic law the index *p* and the cubic law the index *c*.

Figure 2 shows the results of the TGA. The upper graph shows the TGA curves for all the samples studied. The samples at 700 °C differ from the others, their final weight gain being 20.62 mg·cm^{-2} in the soft-annealed state and 14.10 mg·cm^{-2} in the quenched and tempered state. Since the weight gain for all other samples did not exceed 0.85 mg·cm^{-2}, the scale on the Y-axis was reduced to 2.0 mg·cm^{-2} in the following two graphs (**Figures 2b** and **2c**). The red rectangle in **Figure 2a** marks the enlarged area in **Figure 2b**, where the fluctuations on the TGA curves are visible, which are most pronounced on the TGA curves at 400 °C and 500 °C. As shown for the H11 steel[27], this is probably due to the oxidation of the $M_{23}C_6$ ($Cr_{23}C_6$) carbides. The above effect decreases with increasing oxidation temperature. However, as far as the kinetics are concerned, this does not have much influence on the expressed equations, as the TGA curves were fitted with mathematical functions and the range of fluctuations is also less than 0.1 mg·cm^{-2}. The blue rectangle in **Figure 2b** marks the area shown enlarged in the graph on the right (**Figure 2c**), where the scale on the X-axis has been reduced to 10 h. This is to show the difference between the shape of the TGA curves obtained from the heating segment (first part of the TGA curve) and under isothermal conditions (second part of the TGA curve).

Table 2 shows the change in weight for each part of the TGA curve. This is a good indicator of whether the oxide layer formed during the heating segment is sufficient to protect the steel from further oxidation during the isothermal segment. When the weight starts to decrease, it means that carbide oxidation has started, as demonstrated in a previous study.[27] This happens in the temperature range 400–600 °C in both the soft-annealed and quenched-and-tempered states. If the weight does not change significantly, this means that an oxide layer has formed during the isothermal segment, protecting the steel from further oxidation. If the weight increases, as it does at 700 °C (in both states), this means that the steels continue to oxidise during the isothermal segment. Furthermore, as already shown, the oxidation of $M_{23}C_6$ is the cause of the fluctuations at lower temperatures.

Table 2: Weight changes in % for each part of the TGA curve

	TGA (%)		
Temperature (°C)	Part of the TGA curve	Dievar	Dievar-HT
400	1.	0.176	0.174
	2.	0.065	0.107
500	1.	0.197	0.183
	2.	0.163	0.022
600	1.	0.238	0.198
	2.	0.131	0.025
700	1.	0.196	0.252
	2.	3.922	2.664

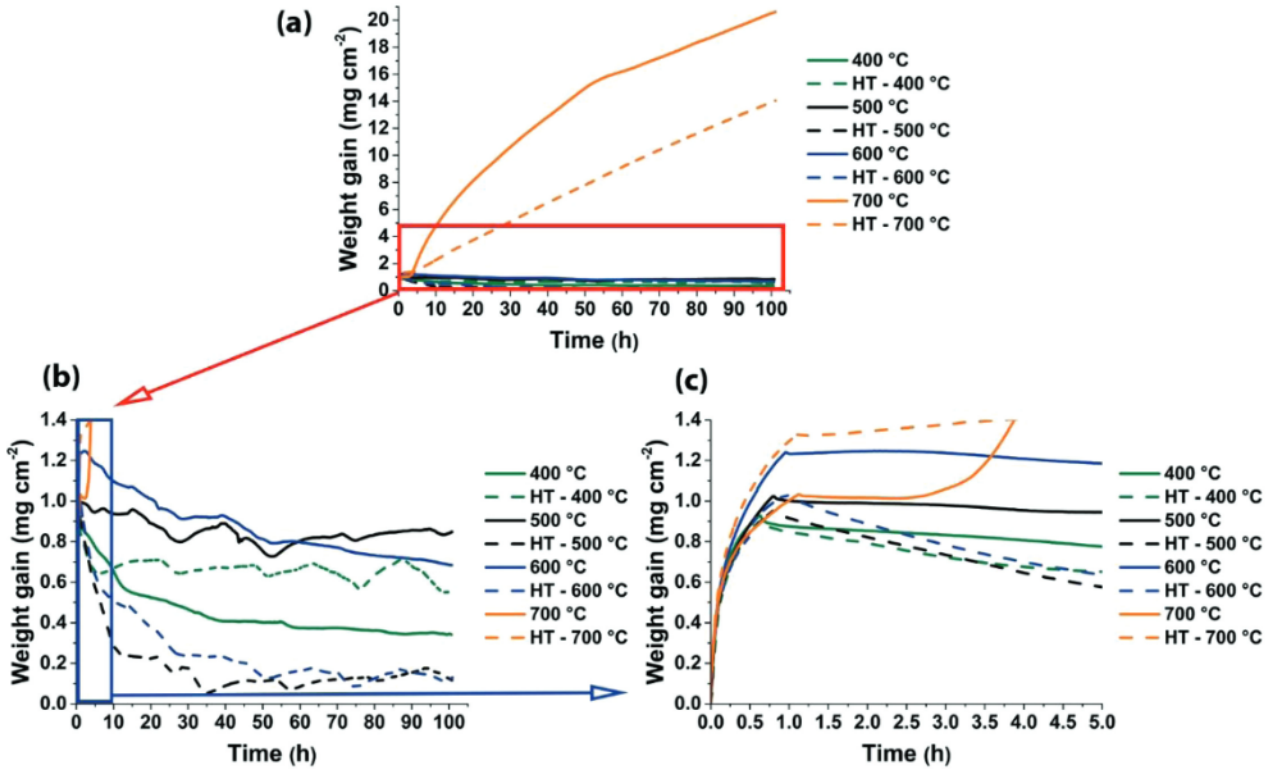

Figure 2: TGA results for all the investigated samples of Dievar hot-work tool steel

The coefficients with the corresponding equation type for each part of the TGA curve can be found below in **Table 3**.

Since fluctuations occur, some of the rate constants for the second part of the TGA curve in **Table 4** have a negative value. The reason for this, as already mentioned, is the decrease in weight during the isothermal segment.

3.3 Microscopy

The microstructures after high-temperature oxidation at a certain temperature and the corresponding initial microstructures are shown in **Figure 3**. The initial microstructures in the soft-annealed condition consist of a ferrite matrix (severely tempered martensite) and spherical carbides. After oxidation at 400 °C, the microstructure consists mainly of ferrite and spherical carbides. The hardness (**Table 5**) decreases, mainly due to Ostwald ripening of the spherical carbides, as the growth reduces the effect of precipitation hardening. The microstructure after oxidation at (400, 500, 600 and 700) °C (**Figure 3**) is almost the same and consists of a ferrite matrix and spherical carbides, which is also reflected in the hardness (**Table 5**). The hardness decreases with increasing temperature due to Ostwald ripening of the carbides.

The microstructures of the heat treated (HT) samples (quenched and tempered) in the initial state and after high-temperature oxidation are shown in **Figure 4**. The initial microstructure consists of tempered martensite and carbides. The microstructure after oxidation at 400 °C and 500 °C is the same as the initial microstructure, indicating that the microstructure is stable in this temperature range. This is also confirmed by the hardness (**Table 5**). The reason that the microstructure is

Table 3: Coefficients are given with the corresponding type of equation for each part of the TGA curve of the samples investigated

Temperature (°C)	Sample	Part of the TGA curve	Equation type	Coefficients				
				A	B	C	D	E
400	Dievar	1.	exponential	–0.39	–171.0	–0.61	–1172.34	1.01
		2.	exponential	0.42	–37891.84	0.21	–205583.31	0.31
	Dievar HT	1.	exponential	–0.48	–218.87	–0.71	–1904.63	1.12
		2.	parabolic	0.70	$-2.22\cdot10^{-7}$	$-3.94\cdot10^{-15}$	/	/
500	Dievar	1.	exponential	–0.45	–187.71	–0.82	–2288.70	1.26
		2.	parabolic	1.00	$-1.8\cdot10^{-6}$	$4.09\cdot10^{-12}$	/	/
	Dievar HT	1.	exponential	–0.46	–192.71	–0.63	–1717.23	1.07
		2.	exponential	0.42	–13817.42	0.57	–32747.42	0.12
600	Dievar	1.	exponential	–0.44	–199.86	–1.06	–2607.38	1.53
		2.	cubic	1.25	$-4.05\cdot10^{-6}$	$1.22\cdot10^{-11}$	$-1.49\cdot10^{-17}$	/
	Dievar HT	1.	exponential	–0.47	–192.97	–0.70	–2164.53	1.18
		2.	exponential	0.55	–5507.25	0.66	–68904.55	0.13
700	Dievar	1.	exponential	–0.40	–172.02	–0.57	–1302.44	0.99
		2.	cubic	0.48	$1.27\cdot10^{-4}$	$-3.31\cdot10^{-10}$	$3.7\cdot10^{-16}$	/
	Dievar HT	1.	exponential	–0.46	–213.85	–0.99	–2247.02	1,49
		2.	parabolic	0.96	$3.99\cdot10^{-5}$	$-1.03\cdot10^{-11}$	/	/

Table 4: Rate constants are given for each part of the TGA curve for the samples studied with the corresponding equation type

Temperature (°C)	Sample	Part of the TGA curve	Equation type	Rate constants		
				k_e/(mg^e·cm^{-2e}·s^{-1})	k_p/(mg^2·cm^{-4}·s^{-1})	k_c/(mg^3·cm^{-6}·s^{-1})
400	Dievar	1.	exponential	$3.724\cdot10^{-4}$	/	/
		2.	exponential	$-9.228\cdot10^{-7}$	/	/
	DievarHT	1.	exponential	$3.549\cdot10^{-4}$	/	/
		2.	parabolic	/	$-2.93\cdot10^{-7}$	/
500	Dievar	1.	exponential	$3.772\cdot10^{-4}$	/	/
		2.	parabolic	/	$7.393\cdot10^{-8}$	/
	DievarHT	1.	exponential	$3.052\cdot10^{-4}$	/	/
		2.	exponential	$-4.173\cdot10^{-7}$	/	/
600	Dievar	1.	exponential	$5.376\cdot10^{-4}$	/	/
		2.	cubic	/	/	$-1.349\cdot10^{-6}$
	DievarHT	1.	exponential	$3.303\cdot10^{-4}$	/	/
		2.	exponential	$-7.404\cdot10^{-7}$	/	/
700	Dievar	1.	exponential	$3.16\cdot10^{-4}$	/	/
		2.	cubic	/	/	$4.54\cdot10^{-2}$
	DievarHT	1.	exponential	$5.83\cdot10^{-4}$	/	/
		2.	parabolic	/	$6.16\cdot10^{-4}$	/

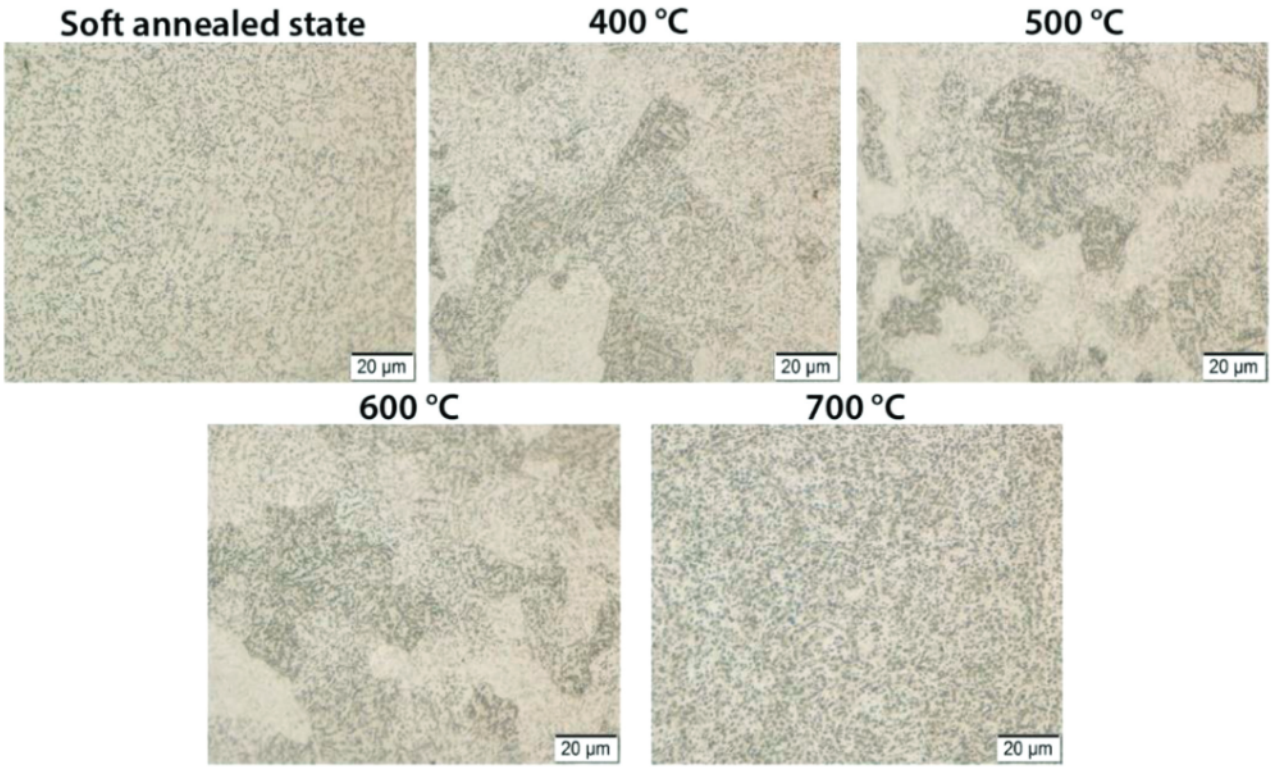

Figure 3: Microstructure of hot-work tool steel Dievar in the soft annealed state in the initial state and after oxidation at (400, 500, 600 and 700) °C for 100 h

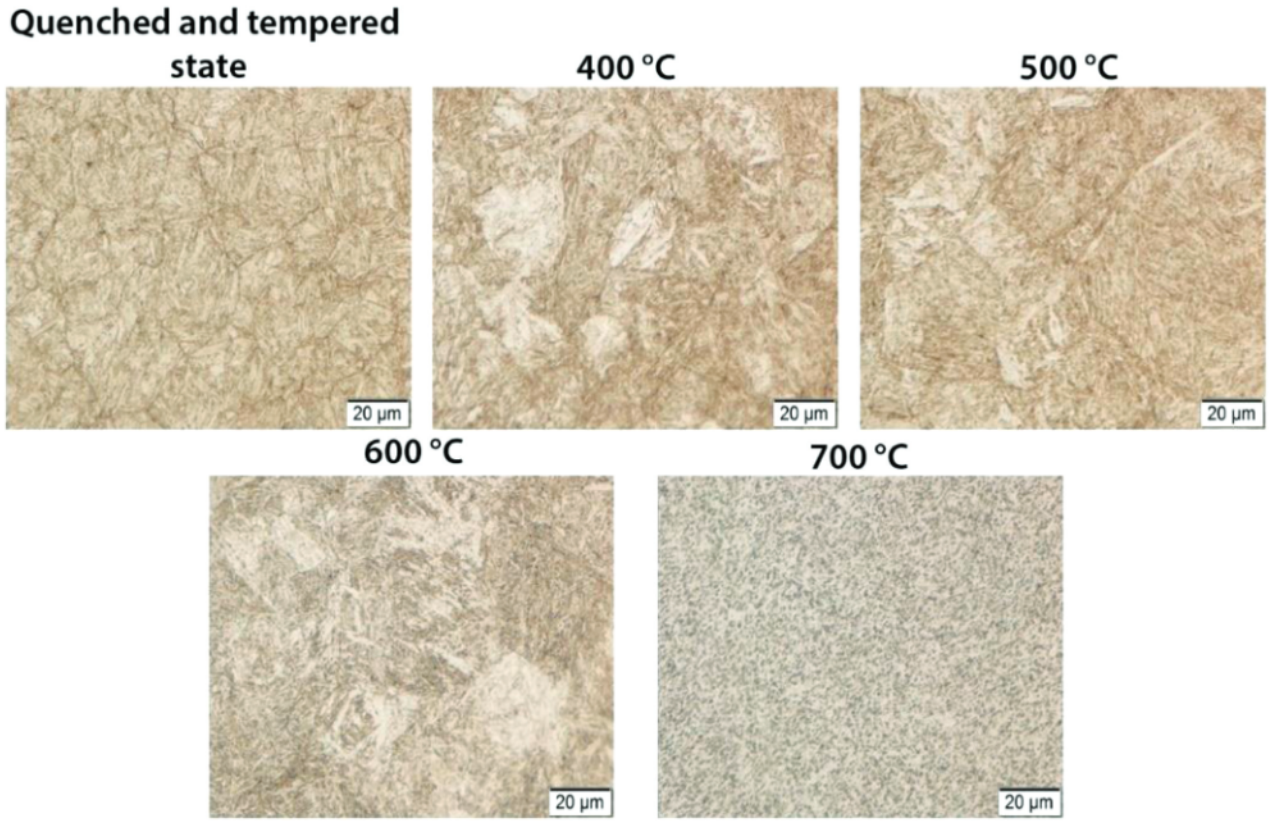

Figure 4: Microstructure of hot-work tool steel Dievar in the quenched-and-tempered state in the initial state and after oxidation at (400, 500, 600 and 700) °C for 100 h

stable is due to the tempering, as the second tempering took place at a temperature of 630 °C. After oxidation at 600 °C, there is additional softening, which leads to a decrease in hardness (**Table 5**). The microstructure still consists of martensite and carbides, but compared to the previous samples, there are a few more carbides that precipitate during the oxidation annealing. The microstructure after oxidation annealing at 700 °C consists of a ferrite matrix and spherical carbides. The reason for this is that the temperature is already in the range of spheroidization annealing. Overall, this can also be seen in the results of the hardness (**Table 5**), which decreases drastically and is comparable to the soft-annealed sample (**Table 5**), whereby the difference is only 15 HV 10.

Table 5: Measured hardness of the hot-work tool steel Dievar in the soft-annealed (Dievar) and quenched-and-tempered (Dievar-HT) states before and after oxidation

Sample	Hardness (HV 10)				
	Before oxidation	After oxidation			
		400 °C	500 °C	600 °C	700 °C
Dievar	198	181	157	162	159
Dievar-HT	440	445	453	301	213

As far as the thickness of the oxide layers is concerned, in most cases a thicker oxide layer is formed in the soft-annealed samples, as can be seen from **Figure 5** and the average of the measured thicknesses of the oxide layers (**Table 6**). At 400 °C, the oxide layer on the soft-annealed sample was 2.3-µm thicker than on the quenched-and-tempered sample. At 500 °C it was about the same thickness, only 0.3 µm thicker on the quenched-and-tempered sample. However, at 600 °C, the oxide layer that formed on the quenched and tempered sample was 6.9 µm thicker than the oxide layer on the soft-annealed sample. On the other hand, the oxide layer on the soft-annealed sample was 40.4 µm thicker at 700 °C.

Table 6: Thickness of the oxide layer formed on Dievar hot-work tool steel in the soft-annealed (Dievar) and quenched-and-tempered (Dievar-HT) states after high-temperature oxidation at (400, 500, 600 and 700) °C

Temperature (°C)	Thickness of the oxide layer (µm)	
	Dievar	Dievar-HT
400	2.7	0.4
500	4.9	5.2
600	3.9	10.8
700	205.1	164.7

From the results collected some general considerations can be made about the behaviour of high-temperature oxidation of the steel studied. As proved by thermodynamic calculations and metallographic analyses, large spherical carbides $(Cr, Mo, Fe)_{23}C_6$, $(Mo, Fe, V)_6C$, VC and some TiCN are present in the steel in the case of a soft-annealed sample within ferrite matrix. The microstructure of the quenched-and-tempered sample is different as it consists of a martensitic matrix and primary (VC and TiCN) and secondary carbides ($(Cr, Mo, Fe)_{23}C_6$ and $(Mo, Fe, V)_6C$). Most are secondary carbides and smaller than the others because they precipitate during the tempering process. For both conditions (soft annealed and quenched and tempered), the transformation of $(Mo, Fe, V)_6C$ to $(Mo, V, Cr)_2C$, which starts at 549 °C and ends at 633 °C, must also be considered. The oxidation kinetics (**Figure 2**) during heating (part 1) shows in all cases the beginnings of following the parabolic or cubic law (best described by the exponential growth function), but under isothermal conditions (part 2) the slope of the TGA curves starts to fall, except at 700 °C. As can be seen from the results, an oxide layer forms during heating. As the oxidation temperature increases, the oxide layer becomes thicker, mainly due to faster diffusion. The weight increases on average from 0.7 mg at 400 °C to 1.1 mg at 700 °C. The reason for this is that oxidation of both the matrix and the alloying elements as well as the carbides takes place simultaneously during heating. It depends on the oxide layer formed whether it protects the steel from further oxidation.

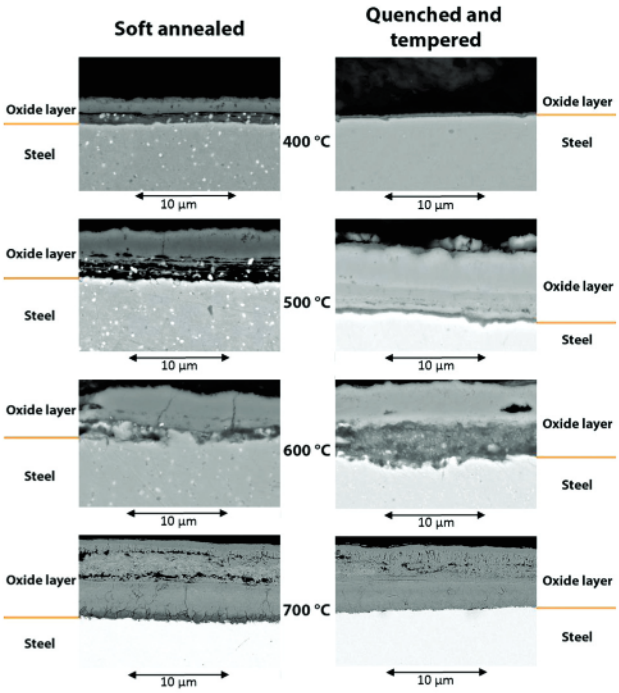

Figure 5: Dievar hot-work tool steel in the soft annealed and quenched and tempered state and the oxide layer formed after high-temperature oxidation at (400, 500, 600 and 700) °C

In the transition from heating to the isothermal part of oxidation, it is in fact decisive, whether the oxide layer is already in thermodynamic equilibrium with the atmosphere and protects the steel from further oxidation or not. The TGA curves decrease at lower temperatures (400–600 °C) and increase at oxidation temperatures of 700 °C. Here, it depends on what has a greater influence on the oxidation rate or which process controls the oxidation kinetics. On the one hand, there is the oxidation of

the iron matrix and, on the other hand, the oxidation of carbides and other alloying elements in the matrix. In this case, it is mainly chromium, molybdenum, silicon, and vanadium. At lower temperatures (T < 700 °C), the oxidation of carbides and alloying elements dissolved in the matrix has been shown to have a greater influence on the oxidation kinetics than the oxidation of iron, although the iron concentration in the matrix is highest. Oxidation of the carbides themselves has been reported by several authors.[29–33] The influence of oxidation of $M_{23}C_6$ ($Cr_{23}C_6$) carbides on the high-temperature oxidation behaviour of hot-work tool steel has been analysed in detail using AISI H11 hot-work tool steel as an example.[27] It was found that carbides and surrounding areas (with increased alloying elements) can serve as potential sites for chromium oxide formation. In the case of $Cr_{23}C_6$, the chromium begins to form chromium oxide (Cr_2O_3), which is a product of carbide oxidation.[27] At the same time, oxidation of the carbide itself also produces CO_2,[31] which is also an oxidation product, with the chemical reaction proceeding in Equation (9):

$$\frac{4}{93}Cr_{23}C_6 + O_2 = \frac{46}{93}Cr_2O_3 + \frac{8}{31}CO_2 \qquad (9)$$

Meanwhile, other carbides present MC, M_2C and M_6C do not have much influence on the oxidation behaviour.[27,34] However, it was also found that chromium does not form a single oxide (Cr_2O_3), but rather a spinel-shaped oxide that forms the inner oxide sublayer.[27] The main cause of the TGA curve oscillations (**Figure 2**) is the oxidation of the $M_{23}C_6$ carbides, as CO_2 is the product of carbide oxidation. This means that the local gas volume in the oxide layer increases. At the same time, the expansion coefficients (α) of the individual oxides formed must be taken into account. The CO_2 formed during the oxidation of the carbides leaves the oxide layer, which can be seen on the TGA curve as a slope in the negative direction, because at the same time stresses develop in the oxide layer, which lead to cracks, and part of the oxide falls off. It has been demonstrated by other authors that if the gas produced (CO or CO_2, as in our case) cannot escape through microchannels (micropores and cracks), its pressure starts to increase, leading to the formation of new pores or even cracks or fractures in the oxide layer.[18,27,35] The higher the temperature, the lower the influence of the oxidation of the carbides on the oxidation kinetics of the steel under investigation, which can be seen on the TGA curves (**Figure 2**), as basically no fluctuations are visible at 700 °C.

The fluctuations in the TGA curves are smaller for soft-annealed samples due to the large spherical carbides and the lower content of alloying elements in the matrix. It has been shown[15,27,36] that oxidation is more continuous with larger carbides and consequently the oxide layer is thicker.

4 CONCLUSIONS

The oxidation kinetics are influenced by the heat treatment of the steel. In general, the oxidation kinetics of the quenched-and-tempered samples are slower than the oxidation kinetics of the soft-annealed samples. Smaller differences only occur at temperature of 400 °C. This is largely influenced by the alloying elements dissolved in the matrix. In the quenched-and-tempered samples, more alloying elements are dissolved and consequently the oxide layer formed is denser, which prevents any further diffusion of iron and oxygen.

The oxidation of $Cr_{23}C_6$ carbides causes stresses in the oxide layer, which leads to pores and cracks, but can also cause the oxide layer to crumble. The higher the temperature, the smaller the effect, as the diffusion is already so fast that the oxidation of the carbides no longer affects the oxidation kinetics of the steel, so that even $Cr_{23}C_6$ carbides ($\geq$ 700 °C) begin to slowly dissolve into the oxide layer at higher temperatures. Other carbides present, however, have no significant influence on the oxidation.

5 REFERENCES

[1] G. Roberts, G. Krauss, R. Kennedy, Tool Steels, 5th ed., ASM International, Materials park 1998, 364

[2] R. A. Mesquita, Tool steels: properties and performance, 1st ed., CRC Press, Boca Raton 2016, 257

[3] F. Qayyum, M. Shah, S. Manzoor, M. Abbas, Comparison of thermomechanical stresses produced in work rolls during hot and cold rolling of cartridge brass 1101, Mater. Sci. Technol., 31 (**2015**) 3, 317–324, doi:10.1179/1743284714Y.0000000523

[4] A. Medvedeva, J. Bergström, S. Gunnarsson, J. Andersson, High-temperature properties and microstructural stability of hot-work tool steels, Mater. Sci. Eng. A, 523 (**2009**) 1–2, 39–46, doi:10.1016/j.msea.2009.06.010

[5] R. Markežič, N. Mole, I. Naglič, R. Šturm, Time and temperature dependent softening of H11 hot-work tool steel and definition of an anisothermal tempering kinetic model, Mater. Today Commun., 22 (**2020**) 100744, 1–7, doi:10.1016/j.mtcomm.2019.100744

[6] D. Caliskanoglu, I. Siller, R. Ebner, H. Leitner, W. Waldhauser, F. Jeglitsch, Thermal Fatigue and Softening Behavior of Hot Work Tool Steels, Proc. 6th Int. Tool. Conf., Karlstad 2002, 707–719

[7] Q. Zhou, X. Wu, N. Shi, J. Li, N. Min, Microstructure evolution and kinetic analysis of DM hot-work die steels during tempering, Mater. Sci. Eng. A, 528 (**2011**) 18, 5696–5700, doi:10.1016/j.msea.2011.04.024

[8] Z. Zhang, D. Delagnes, G. Bernhart, Microstructure evolution of hot-work tool steels during tempering and definition of a kinetic law based on hardness measurements, Mater. Sci. Eng. A, 380 (**2004**) 1–2, 222–230, doi:10.1016/j.msea.2004.03.067

[9] A. Jilg, T. Seifert, Temperature dependent cyclic mechanical properties of a hot work steel after time and temperature dependent softening, Mater. Sci. Eng. A, 721 (**2018**), 96–102, doi:10.1016/j.msea.2018.02.048

[10] N. Mebarki, D. Delagnes, P. Lamesle, F. Delmas, C. Levaillant, Relationship between microstructure and mechanical properties of a 5% Cr tempered martensitic tool steel, Mater. Sci. Eng. A, 387–389 (**2004**), 171–175, doi:10.1016/j.msea.2004.02.073

[11] S. D. Cramer, B. S. Covino Jr, ASM Handbook Volume 13B: Corrosion: Materials, ASM International, Materials park 2005, 704

[12] T. J. A. Richardson, Shreir's Corrosion, 1st ed., Elsevier Science, Amsterdam 2009, 4000

[13] G. Y. Lai, High-Temperature Corrosion And Materials Applications, ASM International, Materials park 2007, 461

[14] R. W. Revie, Uhlig's Corrosion Handbook, 3rd ed., John Wiley & Sons, Inc, Hoboken (New Jersey) 2011, 1296

[15] D. J. Young, High Temperature Oxidation and Corrosion of Metals, 1st ed., Elsevier Science, Amsterdam 2008, 592

[16] B. N. Popov, Corrosion Engineering: Principles and Solved Problems, Elsevier, Amsterdam 2015, 792

[17] P. Pedeferri, Corrosion Science and Engineering, Springer, Cham 2018, 720

[18] R. Y. Chen, W. Y. D. Yeun, Review of the High-Temperature Oxidation of Iron and Carbon Steels in Air or Oxygen, Oxid. Met., 59 (**2003**), 433–468, doi:10.1023/A:1023685905159

[19] N. B. Pilling, R. E. Bedworth, Oxidation of metals at high temperatures, J. Inst. Met., 29 (**1923**), 529–539

[20] D. Caplan, G. I. Sproule, R. J. Hussey, Comparison of the kinetics of high-temperature oxidation of Fe as influenced by metal purity and cold work, Corros. Sci., 10 (**1970**) 1, 9–17, doi:10.1016/S0010-938X(70)80093-2

[21] W. E. Boggs, R. H. Kachik, The Oxidation of Iron-Carbon Alloys at 500°C, J. Electrochem. Soc., 116 (**1969**) 4, 424–430, doi:10.1149/1.2411889

[22] D. Caplan, M. Cohen, Effect of cold work on the oxidation of iron from 400-650 °C, Corros. Sci., 6 (**1966**) 7, 321–326, doi:10.1016/S0010-938X(66)80039-2

[23] M. H. Davies, M. T. Simnad, C. E. Birchenall, On the Mechanism and Kinetics of the Scaling of Iron, Jom, 3 (**1951**), 889–896, doi:10.1007/BF03397397

[24] M. H. S. Bidabadi, S. Chandra-ambhorn, A. Rehman, Y. Zheng, C. Zhang, H. Chen, Z-G. Yang, Carbon depositions within the oxide scale and its effect on the oxidation behavior of low alloy steel in low (0.1 MPa), sub-(5 MPa) and supercritical (10 MPa) CO_2 at 550 °C, Corros. Sci., 177 (**2020**), 108950, doi:10.1016/j.corsci.2020.108950

[25] X. Zhang, X. Jie, L. Zhang, S. Luo, Q. Zheng, Improving the high-temperature oxidation resistance of H13 steel by laser cladding with a WC/Co-Cr alloy coating, Anti-Corrosion Methods Mater., 63 (**2016**) 3, 171–176, doi:10.1108/ACMM-11-2015-1606

[26] Y. Min, X. Wu, R. Wang, L. Li, L. Xu, Prediction and analysis on oxidation of H13 hot work steel, J. Iron Steel Res. Int., 13 (**2006**) 1, 44–49, doi:10.1016/S1006-706X(06)60025-3

[27] T. Balaško, M. Vončina, J. Burja, B. Š. Batič, J. Medved, High-temperature oxidation behaviour of AISI H11 tool steel, Metals (Basel), 11 (**2021**) 5, 758, doi:10.3390/met11050758

[28] Thermo-Calc Software, TCFE10: TCS Steel and Fe-alloys Database, Thermo-Calc AB, Stockholm 2019

[29] Z. Ye, P. Wang, D. Li, Y. Li, $M_{23}C_6$ precipitates induced inhomogeneous distribution of silicon in the oxide formed on a high-silicon ferritic/martensitic steel, Scr. Mater., 97 (**2015**), 45–48, doi:10.1016/j.scriptamat.2014.10.028

[30] Y. Gong, D. J. Young, Y. L. Chiu, H. Larsson, A. Shin, J. M. Pearson, M. P. Moody, R. C. Reed, On the breakaway oxidation of Fe9Cr1Mo steel in high pressure CO_2, Acta Mater., 130 (**2017**), 361–374, doi:10.1016/j.actamat.2017.02.034

[31] K. H. Jung, S. J. Kim, Role of $M_{23}C_6$ carbide on the corrosion characteristics of modified 9Cr-1Mo steel in N_2-O_2-CO_2-SO_2 atmosphere at 650 °C, Appl. Surf. Sci., 483 (**2019**), 417–424, doi:10.1016/j.apsusc.2019.03.272

[32] S. Wu, Y. Fei, B. Guo, L. Jing, Corrosion of $Cr_{23}C_6$ coated Q235 steel in wet atmospheres containing Na_2SO_4 at 750°C, Corros. Sci., 100 (**2015**), 306–310, doi:10.1016/j.corsci.2015.08.008

[33] Z. Li, G. Cao, F. Lin, C. Cui, H. Wang, Z. Liu, Phase transformation behavior of oxide scale on plain carbon steel containing 0.4 wt.% Cr during continuous cooling, ISIJ Int., 58 (**2018**) 12, 2338–2347, doi:10.2355/isijinternational.ISIJINT-2018-365

[34] H. J. Grabke, M. Spiegel, A. Zahs, Role of alloying elements and carbides in the chlorine-induced corrosion of steels and alloys, Mater. Res., 7 (**2004**) 1, 89–95, doi:10.1590/S1516-14392004000100013

[35] K. Sachs, J. R. Brown, A theory of decarburization by scale, J. iron steel Inst., 190 (**1958**), 169–170

[36] L. B. Susanto, D. J. Young, Effect of carbide volume fraction on the oxidation of austenitic Fe-Cr-C alloys, Mater. Corros., 57 (**2006**) 6, 467–475, doi:10.1002/maco.200503945